Journal of the European Ceramic Society 22 (2002) 1329–1337

www.elsevier.com/locate/jeurceramsoc

Creep property comparisons for ceramic-fibre-reinforced ceramic–matrix composites

B. Wilshire*

Department of Materials Engineering, University of Wales, Swansea, SA2 8PP, UK

Received 21 March 2001; received in revised form 17 August 2001; accepted 19 September 2001

Abstract

The tensile creep and creep fracture properties are analysed for seven different ceramic–matrix composites, reinforced with silicon carbide or alumina fibres. For this broad product range, the processes controlling creep deformation and damage evolution are identified, showing that the longitudinal fibres govern the rates of strain accumulation and crack development, with the matrices and fibre/matrix interfaces influencing the times and strains to failure. © 2002 Elsevier Science Ltd. All rights reserved.

Keywords: Composites; Creep; Fibre-reinforcement; Fracture

1. Introduction

Numerous research programmes have determined the tensile creep properties of the continuous ceramic-fibre-reinforced ceramic–matrix composites (CFCMCs) being developed for high-temperature aerospace applications. In general, the creep characteristics of CFCMCs have then been discussed in terms of the creep rate mismatch ratio (CMR), defined[1] as the ratio of the creep rates of the fibres ($\dot{\varepsilon}_F$) and the matrix ($\dot{\varepsilon}_M$), so that $CMR = \dot{\varepsilon}_F/\dot{\varepsilon}_M$. When the fibres are more creep resistant than the matrix ($CMR < 1$), the main creep damage mechanism is considered to be periodic fibre fracture. Conversely, when the fibres have a lower creep strength than the matrix ($CMR > 1$), matrix cracking is suggested as the dominant process.

This approach has been illustrated,[1] for example, by reference to tensile creep data recorded for two SiC-fibre-reinforced composites, one produced with a hot-pressed silicon nitride matrix (now termed SiC_f/HPSN) and the other with a reaction-bonded silicon nitride matrix (referred to as SiC_f/RBSN). In monolithic form, reaction-bonded Si_3N_4 is more creep resistant[2] than hot-pressed Si_3N_4, consistent with the suggestion that $CMR < 1$ for the SiC_f/HPSN material, whereas $CMR > 1$ for the SiC_f/RBSN product.[1] However, uncertainties over the relative creep strengths of the fibres and the matrices have resulted in even nominally-identical CFCMCs being classified in both the $CMR > 1$ and $CMR < 1$ categories. Thus, for various types of SiC-fibre-reinforced SiC–matrix composites (designated as SiC_f/SiC type materials), one research group has concluded that the creep resistance of the fibres exceeds that of the matrices,[3] while the opposite view has been advocated by other investigators.[4–6]

To resolve this uncertainty, the comparative creep strengths of the fibres and matrices are now considered in relation to the processes governing strain accumulation and damage evolution during tensile creep of a broad range of ceramic–matrix composites, reinforced with either silicon carbide or alumina fibres.

2. Material descriptions

The strength of CFCMCs depends on load transfer to large volume fractions of high-modulus fibres, with weak fibre/matrix interfaces allowing intact fibres to bridge across cracks developing in the ceramic matrices. In the present analysis, the creep properties are compared for seven composites produced not only with different fibre types, volume fractions and architectures but also with different fibre/matrix interfaces and matrices. These products were reinforced

(a) with ~143 μm diameter fibres aligned parallel (0°) to the tensile direction[1] or

* Tel.: +44-1792-295243; fax: +44-1792-295244.
E-mail address: b.wilshire@swansea.ac.uk (B. Wilshire).

0955-2219/02/$ - see front matter © 2002 Elsevier Science Ltd. All rights reserved.
PII: S0955-2219(01)00452-6

(b) with bundles of ~500 fibres (~15 μm diameter) interwoven to form 2D plys, which were stacked and densified to create multilayer samples having fibre arrays oriented at approximately 0/90° to the tensile axis.[3–8]

The methods used to obtain these materials are outlined below, with their distinguishing compositional and microstructural characteristics summarized in Table 1.

2.1. SiC_f/Al_2O_3 and Al_2O_3 $_f$/SiC composites

The SiC-fibre-reinforced Al_2O_3–matrix composite[3] (referred to as SiC_f/Al_2O_3) was manufactured with satin-woven bundles of Nicalon™ NLM 202 fibres (Nippon Carbon). Initially, the multilayer fibre preforms were processed to coat the fibres with thin boron nitride layers, before ~5 μm thick SiC coatings were deposited by chemical vapour infiltration (CVI), resulting in double BN/SiC interfaces. Finally, the porous alumina matrix was introduced by in situ directional oxidation of liquid aluminium.[9,10]

The alumina-fibre-reinforced SiC–matrix product[7,8] (termed Al_2O_{3f}/SiC) was made with plain-woven bundles of alumina fibres,[11] containing ~85 wt.% γ-alumina and ~15 wt.% amorphous silica (Sumitomo Chemicals). The fibres were coated with a carbon interface layer (~0.5 μm thick), before the porous SiC matrix was formed by chemical vapour infiltration.

2.2. SiC_f/SiC type composites

Three types of SiC-fibre-reinforced SiC–matrix composites have been considered, now referred to as standard SiC_f/SiC,[3] enhanced SiC_f/SiC[5] and $HNSiC_f$/SiC.[6] In all cases, the SiC fibres were carbon coated before the fibre preforms were CVI densified to obtain the polycrystalline SiC matrices. However, several key differences between these three SiC_f/SiC type composites should be noted.

(a) The standard SiC_f/SiC and enhanced SiC_f/SiC products were both reinforced with plain woven arrays of Nicalon™ NLM 202 fibres, whereas the $HNSiC_f$/SiC samples were produced with satin-woven bundles of Hi-Nicalon™ fibres. Standard Nicalon™ fibres contain a silicon oxycarbide ($SiC_{0.85}O_{0.15}$) phase,[12] which causes a loss of creep strength during prolonged exposure at high temperatures. This amorphous phase can be eliminated by electron irradiation under vacuum, giving Hi-Nicalon™ fibres with a higher modulus and better long-term creep strength than Nicalon™ NLM 202 fibres.[13,14]
(b) Carbon interfaces are prone to oxidation during creep at elevated temperatures. Hence, the enhanced SiC_f/SiC and $HNSiC_f$/SiC products were manufactured with 'enhanced' SiC matrices containing boron-based particulate additives. These particles react with oxygen penetrating into the material during creep exposure, forming a sealant glass to limit the rates of oxygen ingress.[15]

2.3. SiC_f/Si_3N_4 type composites

Creep property values have also been published[1] for the two SiC-fibre-reinforced composites produced with either hot-pressed or reaction-bonded silicon nitride matrices, designated as SiC_f/HPSN and SiC_f/RBSN respectively (Table 1). Both products were uniaxially reinforced with SCS-6 fibres, formed by chemical vapour deposition of β-SiC onto 33 μm diameter carbon-fibre cores, giving fibres with an overall diameter of ~143 μm.[16]

Table 1
Distinguishing features of fibre-reinforced composites[a]

Material designation	Fibre type	Fibre diameter (μm)	Fibre structure	Fibre vol.%	Matrix material	Matrix porosity (%)	Interface type	Interface thickness (μm)	Ref.
SiC_f/Al_2O_3	Nicalon™ NLM 202	~15	0/90° satin	38	Al_2O_3	~15	BN/SiC	~5	3
Al_2O_{3f}/SiC	Al_2O_3	~15	0/90° plain	40	SiC	>20	Carbon	~0.5	7
Standard SiC_f/SiC	Nicalon™ NLM 202	~15	0/90° plain	38	SiC	~15	Carbon	<0.5	3
Enhanced SiC_f/SiC	Nicalon™ NLM 202	~12	0/90° plain	40	Enhanced SiC	~15	Carbon	~0.5	5
$HNSiC_f$/SiC	Hi-Nicalon™	~12	0/90° satin	40	Enhanced SiC	~15	Carbon	<0.5	6
SiC_f/HPSN	SCS-6	~143	0°	30	HPSN	~3	–	–	1
SiC_f/RBSN	SCS-6	~143	0°	24	RBSN	30±5	–	–	1

[a] The SiC_f/Al_2O_3 and the three SiC_f/SiC type composites were manufactured by Dupont Lanxide Composites (now Allied Signal), whereas the Al_2O_{3f}/SiC material was specially produced by SEP (Etablissement de Bordeaux, France). The SiC_f/HPSN was made by Textron Speciality Materials, using Stark LC-12 Si_3N_4 powder (with 5 wt.% Y_2O_3 and 1.25 wt.% MgO as sintering additions) which was hot-pressed at 30 MPa and 1973 K. The SiC_f/RBSN was fabricated at the NASA-Lewis Research Centre, USA. It should also be noted that, while the diameters of the fibres reinforcing the enhanced SiC_f/SiC and $HNSiC_f$/SiC products have been quoted as ~12 μm,[5,6] the diameters of the Nicalon™ and Hi–Nicalon™ fibres supplied by Nippon Carbon are normally ~15 μm.

3. Experimental observations

The present study analyses results available from tensile creep tests completed at 1300 °C for the six composites reinforced with various types of SiC fibres (Table 1). However, with the alumina fibres reinforcing the Al_2O_{3f}/SiC specimens, a transformation to mullite occurs above 1127 °C, so the maximum creep temperature was limited to 1100 °C.[7,8] For the SiC_f/Al_2O_3 material,[3] the three SiC_f/SiC type composites[3,5,6] and the SiC_f/HPSN samples,[1] the creep tests were carried out in air, whereas the SiC_f/RBSN was tested under a nitrogen atmosphere[1] and the Al_2O_{3f}/SiC product was tested under vacuum.[7,8]

With the SiC_f/Al_2O_3 and the three SiC_f/SiC type composites, a normal primary stage was observed during which the creep rate decayed continuously with time towards a minimum value, with little or no secondary or tertiary stages apparent before fracture. Continuously decaying primary curves were also reported for the uniaxially-reinforced SiC_f/HPSN and SiC_f/RBSN specimens, but the tests were discontinued before failure took place,[1] recording the creep rates attained after 100 h, i.e. values close to the minimum rates expected for the imposed creep conditions. In contrast, with the Al_2O_{3f}/SiC testpieces, a decaying primary stage of relatively short duration was followed immediately by an extended tertiary period, during which the creep rate accelerated until fracture occurred.

3.1. Creep data comparisons

The stress/creep rate relationships in Fig. 1 allow the minimum creep rates recorded for the SiC_f/Al_2O_3 product[3] to be compared at 1300 °C with data obtained

(a) for an alumina-matrix composite reinforced with 25 vol.% of dispersed SiC whiskers[17] and
(b) for Nicalon™ fibres.[18]

The incorporation of SiC whiskers significantly increases the creep resistance of alumina,[17] so the porous alumina matrix of the fibre-reinforced SiC_f/Al_2O_3 samples must have a creep strength less than that of the fully-dense whisker-reinforced alumina. Yet, at comparable stress levels, the creep rates displayed by the SiC-fibre-reinforced alumina are several orders of magnitude lower than those recorded for the SiC-whisker-reinforced alumina (Fig. 1), so the matrix can make little contribution to the overall creep resistance of the fibre-reinforced SiC_f/Al_2O_3 composite. This conclusion is fully consistent with the observation that the processing operations involved in making the SiC_f/Al_2O_3 material result in the formation of residual-stress-induced microcracks,[19] which reduce the strength of the alumina matrix.

While the creep resistance of the fibres exceeds that of the matrix in the SiC_f/Al_2O_3 composite, $CMR > 1$ behaviour was assumed for the standard SiC_f/SiC product,[4] because the creep rates for SiC samples obtained by chemical vapour deposition[20] appeared to be lower than the rates predicted by extended extrapolation of the creep data for the Nicalon™ fibres.[18] However, the inevitable scatter in the results for Nicalon™ fibres (Fig. 2) does not promote confidence in the accuracy of the extrapolated creep rate values. Moreover, the low creep resistance of CVI-deposited SiC matrices is apparent from the fact that the creep strength of the standard SiC_f/SiC composite is inferior to that of the SiC_f/Al_2O_3 samples at 1300 °C (Fig. 2), even though both composites were reinforced with 0.38 volume fractions of

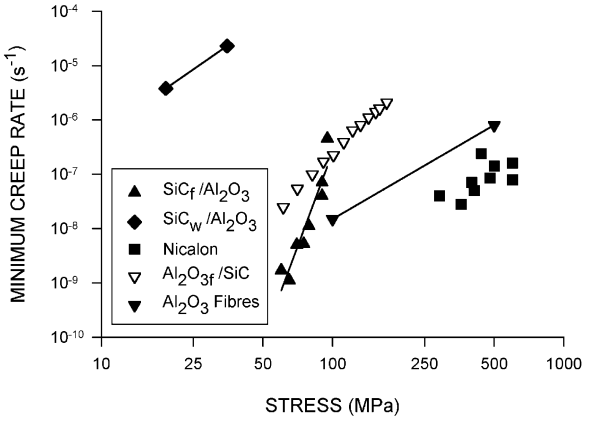

Fig. 1. Comparisons of the stress/minimum creep rate relationships for the SiC-fibre-reinforced alumina-matrix composite (SiC_f/Al_2O_3), the SiC-whisker-reinforced alumina (SiC_W/Al_2O_3) and Nicalon™ fibres at 1300 °C, together with the equivalent data for the Al_2O_{3f}/SiC samples and their reinforcing Al_2O_3 fibres at 1100 °C.

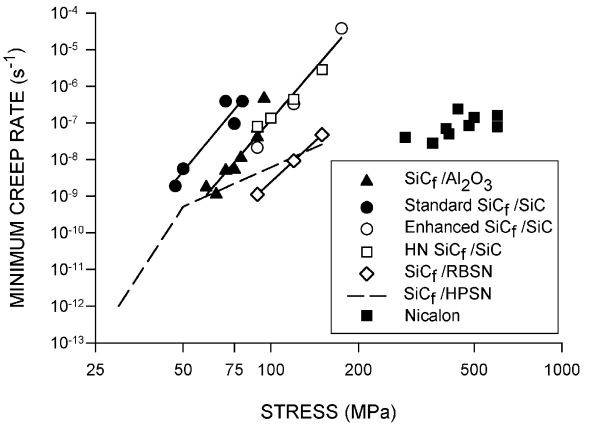

Fig. 2. Comparisons of the stress/minimum creep rate relationships for the SiC_f/Al_2O_3, standard SiC_f/SiC, enhanced SiC_f/SiC, HNSiC_f/SiC, SiC_f/RBSN and SiC_f/HPSN composites in relation to data for Nicalon™ fibres at 1300 °C.

interwoven bundles of ~15 μm diameter Nicalon™ NLM 202 fibres (Table 1). Hence, the porous CVI-deposited SiC matrix of the standard SiC_f/SiC specimens appears to be characterized by a creep resistance at least as poor as that of the weak Al_2O_3 matrix of the SiC_f/Al_2O_3 testpieces.

As with the standard SiC_f/SiC samples,[4] it has been assumed that the enhanced SiC_f/SiC and the $HNSiC_f/SiC$ materials,[5,6] as well as the Al_2O_{3f}/SiC specimens,[7,8] exhibit $CMR > 1$ behaviour.

Yet, the stress/creep rate plots for the enhanced SiC_f/SiC and $HNSiC_f/SiC$ samples are close to that for the SiC_f/Al_2O_3 composite, with a slightly lower creep resistance displayed by the standard SiC_f/SiC product (Fig. 2). Clearly, stresses about five times higher must be applied to the Nicalon™ fibres to obtain creep rates comparable with those observed for the Nicalon™-fibre-reinforced composites at 1300 °C (Fig. 2). Similarly, a near five-fold difference in creep strength is also evident for the Al_2O_{3f}/SiC composite and its reinforcing alumina fibres at 1100 °C (Fig. 1). Since all of these composites contained ~40 vol.% fibres, the fibres parallel to the tensile stress axis occupy about one fifth of the testpiece cross-sectional areas, so the creep properties of the five woven CFCMCs in Table 1 must be governed by the creep resistance of the longitudinal (0°) fibres.

The uniaxially-reinforced $SiC_f/HPSN$ and $SiC_f/RBSN$ composites have been classified[1] as displaying $CMR < 1$ and $CMR > 1$ behaviour, respectively. However, no stress/creep rate data was reported[1] to confirm that the creep strength of the RBSN matrix was superior and the creep resistance of the HPSN matrix was inferior to that of the reinforcing SCS-6 fibres. Moreover, for these statements to be valid, after compensating for differences in fibre volume fraction, plots of the variations of the minimum creep rate ($\dot{\varepsilon}_m$) with stress (σ) for the SCS-6 fibres would have to lie at some intermediate position between the log σ/log $\dot{\varepsilon}_m$ plots for the $SiC_f/HPSN$ and $SiC_f/RBSN$ samples. This option seems unlikely, given the small stress difference between the stress/creep rate relationships for the two 0° CFCMCs (Fig. 2). Furthermore, again allowing for differences in the volume fractions of longitudinal fibres, the log σ/log $\dot{\varepsilon}_m$ plots for the $SiC_f/HPSN$ and $SiC_f/RBSN$ specimens are broadly comparable with the data shown for the four woven SiC-fibre-reinforced products in Fig. 2. On this basis, for the $SiC_f/HPSN$ and $SiC_f/RBSN$ materials, as with the five woven CFCMCs in Table 1, it appears that the creep strengths of the longitudinal fibres determine the rates of creep strain accumulation.

3.2. Creep fracture properties

The creep tests carried out for the five woven CFCMCs in Table 1 were continued to failure, whereas creep rupture properties were not reported for the 0° $SiC_f/HPSN$ and 0° $SiC_f/RBSN$ samples.[1] For clarity, the creep fracture characteristics will, therefore, be analysed initially for the four woven SiC-fibre-reinforced composites, providing a framework for subsequent discussion of the behaviour patterns exhibited by the woven Al_2O_3-fibre-reinforced product.

In line with the stress/creep rate plots in Fig. 2, at 1300 °C, the stress rupture strengths of the enhanced SiC_f/SiC and $HNSiC_f/SiC$ are similar to those of the SiC_f/Al_2O_3 composite, with the standard SiC_f/SiC material displaying inferior creep fracture resistance (Fig. 3). Yet, for all four products (Fig. 4), the rupture life (t_r) increases with decreasing minimum creep rate ($\dot{\varepsilon}_m$), showing that fracture is strain controlled. Thus, with the fibres determining the rates of creep strain accumulation, creep of the longitudinal fibres must also govern the times to failure.

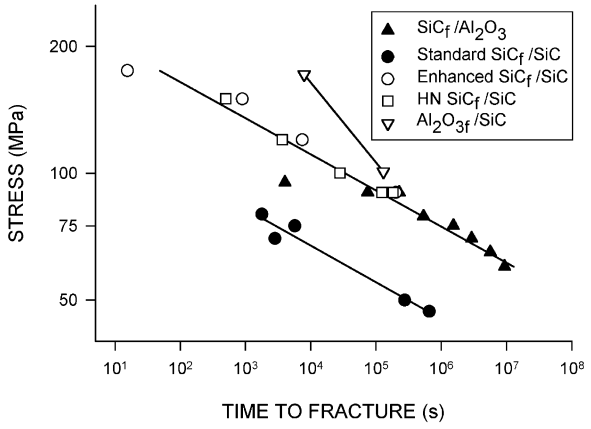

Fig. 3. The variations of the creep rupture life with stress for the SiC_f/Al_2O_3, standard SiC_f/SiC, enhanced SiC_f/SiC and $HNSiC_f/SiC$ composites at 1300 °C and for the Al_2O_{3f}/SiC composite at 1100 °C.

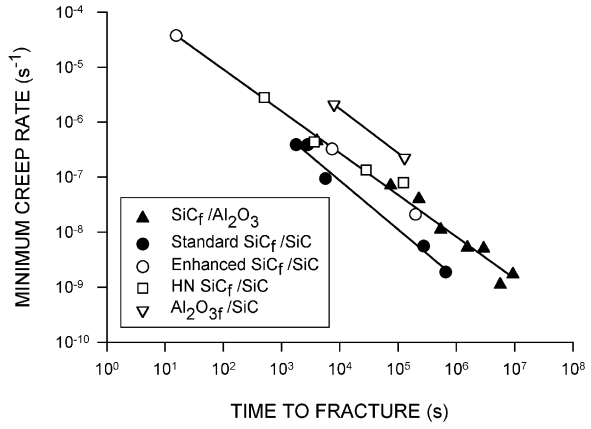

Fig. 4. The dependences of the creep rupture life on the minimum creep rate recorded for the SiC_f/Al_2O_3, standard SiC_f/SiC, enhanced SiC_f/SiC and $HNSiC_f/SiC$ composites at 1300 °C and for the Al_2O_{3f}/SiC composite at 1100 °C.

Analysis of the log $\dot{\varepsilon}_m$/log t_r data in Fig. 4 shows that

$$\dot{\varepsilon}_m.t_r = \text{constant} \quad (1)$$

with $\dot{\varepsilon}_m.t_r \cong 0.001$ for the standard SiC_f/SiC samples. In contrast, with the SiC_f/Al_2O_3 specimens, $\dot{\varepsilon}_m.t_r$ increases with decreasing stress (Fig. 5). It has been shown[3] that this difference in behaviour pattern can be rationalized through the expression

$$\dot{\varepsilon}_m.t_r \cong X\varepsilon_r \quad (2)$$

where X is a constant (with $X \cong 0.5$ at 1300 °C) and ε_r is the total creep strain to failure. Thus, with the standard SiC_f/SiC samples, $\dot{\varepsilon}_m.t_r \cong 0.001$ and $\varepsilon_r \cong 0.002$ over the entire stress range studied whereas, with the SiC_f/Al_2O_3 specimens, $\dot{\varepsilon}_m.t_r$ increased from ~0.001 to ~0.018 as ε_r increased from ~0.002 towards ~0.035 with decreasing applied stress (Figs. 5 and 6). Although actual ductility values were not quoted,[5,6] estimates from published creep curves indicate that $\dot{\varepsilon}_m.t_r$ and ε_r also increase with decreasing stress in tests of more than one hour duration with the enhanced SiC_f/SiC and $HNSiC_f/SiC$ products (Figs. 5 and 6), but longer term results would be needed to verify that these trends match those found[3] for the SiC_f/Al_2O_3 material.

The dependence of $\dot{\varepsilon}_m.t_r$ on ε_r [Eq. (2)] can be explained most easily[3] by describing the changes in creep strain (ε) with time (t), for continuously decaying creep curves, as

$$\varepsilon = at^x \quad (3)$$

where a and x are constants. Differentiation (putting $t = t_r$) then gives Eq. (2), with $x = X \cong 0.5$. Furthermore, by considering the shapes of the creep strain/time curves, differences in the creep and creep fracture properties obtained for the woven SiC-fibre-reinforced composites (Figs. 2 and 3) can be interpreted[3] in terms of the observed variations in ε_r (Fig. 6).

Fig. 7 shows the creep curves recorded under the same test conditions for the standard SiC_f/SiC and enhanced SiC_f/SiC composites.[3,5] Except for the small amounts of boron-based particulates present in the 'enhanced' SiC matrix, these materials are very similar (Table 1). Because the longitudinal fibres control the rates of creep strain accumulation, the initial portions of the creep curves are indistinguishable (with comparable initial curves also occurring[3,6] with the SiC_f/Al_2O_3 and $HNSiC_f/SiC$ samples). However, with the standard SiC_f/SiC product, the ε_r values are low over the entire stress range studied (Fig. 6). Consequently, the creep curves terminate early (Fig. 7), giving high $\dot{\varepsilon}_m$ and low t_r values (Figs. 2 and 3). In contrast, with the enhanced SiC_f/SiC (as well as the SiC_f/Al_2O_3 and $HNSiC_f/SiC$

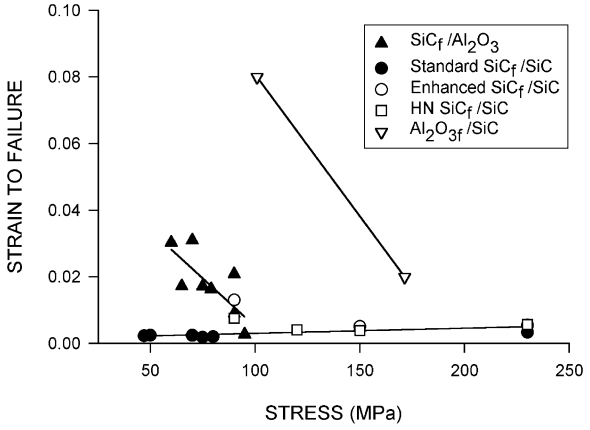

Fig. 6. The stress dependencies of the creep strains to failure for the SiC_f/Al_2O_3, standard SiC_f/SiC, enhanced SiC_f/SiC and $HNSiC_f/SiC$ composites at 1300 °C, together with the creep ductility values for the Al_2O_{3f}/SiC material at 1100 °C.

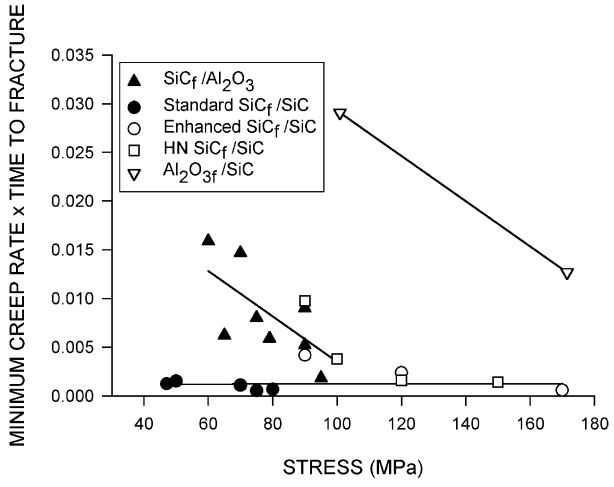

Fig. 5. The stress dependencies of the product of the minimum creep rate and the time to failure for the SiC_f/Al_2O_3, standard SiC_f/SiC, enhanced SiC_f/SiC and $HNSiC_f/SiC$ composites at 1300 °C and for the Al_2O_{3f}/SiC composite at 1100 °C.

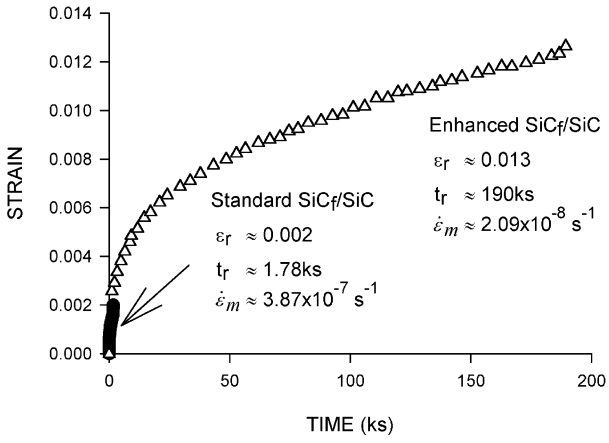

Fig. 7. Creep strain/time curves for the standard SiC_f/SiC and the enhanced SiC_f/SiC composites tested in air at 1300 °C under a stress of 90 MPa.

materials), creep must continue for much longer times when failure occurs at higher ductilities (Fig. 7), resulting in lower minimum creep rates and longer rupture lives (Figs. 2 and 3). The observed differences in ε_r (Fig. 6) can then be explained by considering the processes of creep damage accumulation which lead to fracture of the woven SiC-fibre-reinforced composites.

3.3. Creep damage accumulation

With the SiC_f/Al_2O_3 and the three SiC_f/SiC type composites (Table 1), creep of the longitudinal fibres is accompanied by cracking of the weak brittle matrices (Fig. 8). As the matrix cracks grow mainly perpendicular to the tensile stress axis, by-passing transverse fibres, they eventually become arrested within the longitudinal fibre bundles. The weak fibre/matrix interfaces then allow the cracks to become bridged by unbroken fibres in the longitudinal bundles, with the rate of crack growth determined by creep of the bridging fibres. However, the crack-bridging fibres fail progressively as oxygen penetrates into the testpieces. This results in fracture surfaces with near-planar crack growth zones, characterized by oxidation-assisted in-plane failure of the longitudinal fibres (Fig. 9a), together with regions where sudden failure occurs by fibre pull out (Fig. 9b). Yet, while this general mode of fracture applies to all four woven SiC-fibre-reinforced composites, the susceptibility to oxidation-assisted failure of the crack-bridging SiC fibres differs.

With the standard SiC_f/SiC samples, cracks nucleate preferentially at macropores present in the matrix regions between the interwoven fibre bundles.[3] Neighbouring macropore-nucleated surface cracks link up and grow, with oxygen penetrating directly along the opening crack. Oxidation-assisted failure of the crack-bridging SiC fibres then allows rapid growth of a dominant crack to the size required for sudden propagation by fibre pull out (Fig. 9), resulting in low creep ductilities (Fig. 6).

With the enhanced SiC_f/SiC and $HNSiC_f/SiC$ products, cracks also nucleate at large matrix pores,[5,6] but the boron-based additives in the 'enhanced' matrices produce a sealant glass within the developing cracks, which restricts oxygen penetration.[15] By limiting oxidation-assisted fibre failure, crack growth rates are lower, deferring fracture to higher creep strains (Fig. 7).

Resistance to oxidation-assisted fibre failure, equivalent to that resulting from the formation of a 'sealant glass' in the enhanced SiC_f/SiC and $HNSiC_f/SiC$ samples, is achieved by different mechanisms with the SiC_f/Al_2O_3 composite.[3] In this case, cracks develop extensively throughout the specimen gauge lengths, because the residual-stress-induced microcracks[19] in the as-produced Al_2O_3 matrix allow easy crack nucleation during creep. Indirect oxygen ingress through the micro-cracked Al_2O_3 matrix is then slower than direct penetration along the surface-nucleated cracks formed in the standard SiC_f/SiC specimens.[3] Moreover, the double BN/SiC coatings on the fibres in the SiC_f/Al_2O_3 material are more resistant to oxidation than the carbon fibre coatings in the SiC_f/SiC type products (Table 1). Hence, reduced rates of oxidation-assisted fibre failure and crack growth again postpone failure to higher creep strains (Fig. 6).

With the SiC_f/Al_2O_3 testpieces, examination of the fracture surfaces showed that the area occupied by the near-planar crack growth zones increased and the fractional

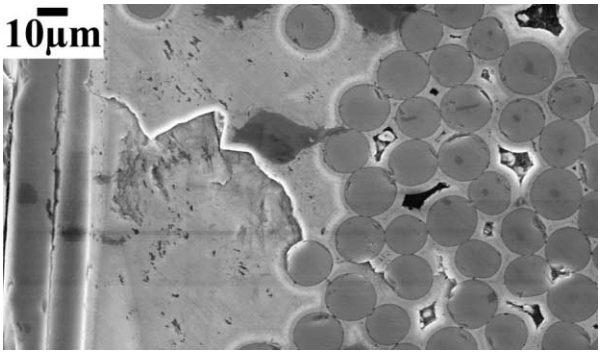

Fig. 8. Scanning electron micrograph showing matrix crack development in the standard SiC_f/SiC composite tested in air at 1300 °C.

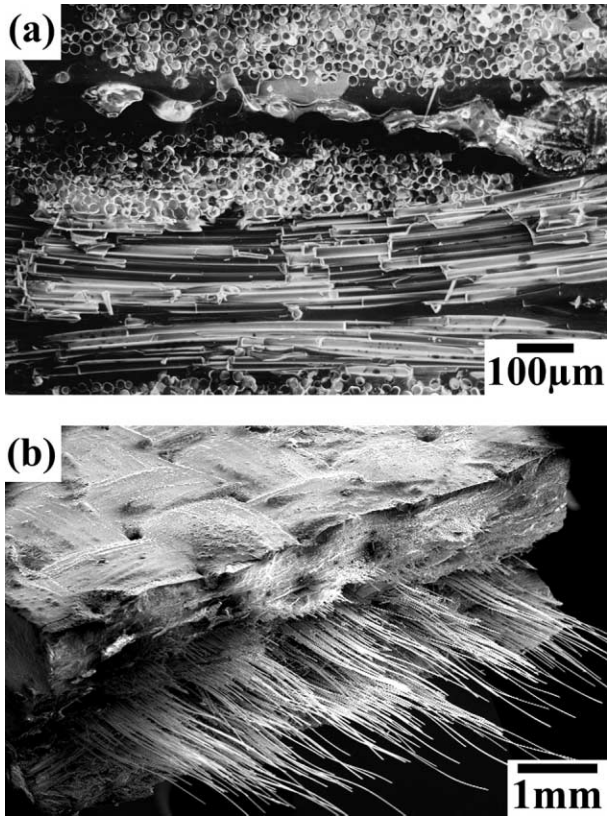

Fig. 9. Scanning electron micrographs showing (a) the crack growth zones characterized by in-plane oxidation-assisted fibre failure and (b) the final fibre pull-out zone on the fracture surface of the standard SiC_f/SiC composite crept to failure in air at 1300 °C.

area of the fibre pull-out decreased with increasing test duration.[3] Thus, at progressively lower creep stresses, creep must continue until the largest planar cracks cause the stresses on the non-cracked regions of the testpiece cross-sections to reach the critical levels necessary for rapid failure by fibre pull out. With the SiC_f/Al_2O_3 composite (and, seemingly, with the enhanced SiC_f/SiC and $HNSiC_f/SiC$ products), the creep ductility therefore increases with decreasing applied stress (Fig. 6).

Many features of the behaviour patterns observed for the woven SiC-fibre-reinforced composites are replicated by the Al_2O_{3f}/SiC product. Thus, the longitudinal fibres determine the rates of creep strain accumulation. Creep of the Al_2O_3 fibres is accompanied by cracking of the porous SiC matrix, with the dependence of t_r on $\dot{\varepsilon}_m$ (Fig. 4) indicating that creep of the 0° fibres again controls the rates of crack development. Furthermore, ε_r increases with decreasing stress (Fig. 6), implying that larger cracks must develop to cause failure at lower stresses, with fracture eventually occurring by progressive fibre failure and, finally, by fibre pull out.[7,8]

4. Discussion

While earlier investigations have suggested that the Al_2O_{3f}/SiC material,[7,8] the three SiC_f/SiC type products[3,5,6] and the $SiC_f/RBSN$ samples[1] display $CMR > 1$ behaviour, the present analysis shows that the creep strengths of the fibres exceed those of the matrices (i.e. $CMR < 1$), so the longitudinal fibres control the rates of creep strain accumulation for all seven CFCMCs in Table 1. Moreover, creep of the longitudinal crack-bridging fibres also governs the rates of crack growth, accounting for the creep rate dependences of the rupture lives. (Fig. 4). Hence, with $CMR < 1$, periodic fibre fracture is the controlling damage process.[1] However, matrix cracking can affect the rates of oxidation-assisted failure of the crack-bridging fibres, influencing the strains and times to fracture.

4.1. Creep of SiC-fibre-reinforced composites

The $SiC_f/HPSN$ and $SiC_f/RBSN$ materials exhibit stress/creep rate properties which are broadly comparable with those observed for the woven SiC-fibre-reinforced products (Fig. 2). For equivalent volume fractions of longitudinal fibres, similar composite creep strengths are therefore displayed over the stress ranges covered at 1300 °C, irrespective of whether uniaxially-aligned SCS-6 fibres or interwoven arrays of Nicalon™ NLM 202 or Hi-Nicalon™ fibres were used for reinforcement.

In this context, it seems surprising that the same UTS values (~230 MPa) and creep strengths were found, even though the enhanced SiC_f/SiC samples[5] were reinforced with plain-woven bundles of Nicalon™ NLM 202 fibres, whereas the $HNSiC_f/SiC$[6] composite contained satin-woven bundles of Hi-Nicalon™ fibres (Table 1). The extent to which the fibres bend under load and the attendant risk of fibre damage should be lower with a satin weave. In addition, creep strength advantages could be anticipated with Hi-Nicalon™ fibres.[21] Unfortunately, the tests carried out for the enhanced SiC_f/SiC and $HNSiC_f/SiC$ samples employed stresses giving maximum creep lives of only ~100 h.[5,6] Hence, low-stress test results are needed to determine the extent to which the use of satin-weave configurations and Hi–Nicalon™ fibres improve long-term creep resistance.

With the woven SiC-fibre-reinforced composites, the rates of creep strain accumulation and crack growth are governed by the creep resistance of the longitudinal Nicalon™ or Hi–Nicalon™ fibres. However, even the latest generations of near-stoichiometric SiC fibres are prone to oxidation at high creep temperatures.[21] Consequently, the ease of oxygen penetration into the specimens as matrix cracking occurs, as well as the susceptibility of the fibres and fibre/matrix interfaces to oxidation, affect the rates of progressive oxidation-assisted failure of the crack-bridging fibres.

With the standard SiC_f/SiC product, direct oxygen penetration along a dominant macropore-nucleated crack leads to rapid oxidation-assisted failure of the carbon-coated crack-bridging fibres, resulting in low creep ductilities (Figs. 6 and 7) and poor creep and creep rupture strengths (Figs. 2 and 3). Superior properties are then achieved with the enhanced SiC_f/SiC and $HNSiC_f/SiC$ testpieces (Figs. 2 and 3), because the boron-based particulates in the 'enhanced' matrices limit oxygen penetration along the developing cracks, reducing the rates of progressive fibre failure to give higher strains and times to fracture (Fig. 7). Equivalent creep and creep rupture properties are also observed for the SiC_f/Al_2O_3 specimens (Figs. 2 and 3), due to the relatively low rates of oxygen ingress through the microcracked Al_2O_3 matrix and the fact that the double BN/SiC interfaces are less susceptible to oxidation than carbon interfaces. Hence, while the fibres control the rates of creep strain accumulation and crack growth, factors which affect both matrix crack development and progressive oxidation-assisted fibre failure must be taken into account to explain the detailed creep and creep fracture properties exhibited by the different woven SiC-fibre-reinforced composites (Table 1).

4.2. Variations in creep curve shape

With the woven SiC-fibre-reinforced samples, the rates of creep strain accumulation are governed by the fibres, but the creep strengths of individual fibres vary, as shown by the scatter in the data for Nicalon™ fibres (Fig. 2). Since the weakest fibre regions deform most

easily, the creep rates are initially high, decreasing as the load is transferred to the stronger fibres. Creep of the fibres is accompanied by cracking of the matrices but, because the porous matrices are weak, matrix cracking has little effect on the small contributions made by the matrices to the overall strengths of the composites. Consequently, the creep rate can continue to decay, even as matrix cracking develops and localized fibre failure occurs. Fracture then takes place when cracks reach a size sufficient to cause sudden failure by fibre pull-out (Fig. 9), terminating the decaying creep curves with no significant periods of secondary or tertiary creep (Fig. 7).

Continuously-decaying creep curves have been observed not only for the woven SiC-fibre-reinforced composites considered in the present study but also for Nicalon™, Hi–Nicalon™ and many other types of SiC fibres.[21] In contrast, with the Al_2O_{3f}/SiC composite reinforced with woven bundles of Sumitomo fibres, the recorded creep curves showed extended tertiary periods before fracture finally occurred.[7,8] While published creep curves were not found for the alumina fibre type produced by Sumitomo Chemicals,[11] tensile creep curves showing clearly-defined tertiary stages have been reported for a variety of alumina fibres[21] and even for monolithic alumina.[22] On this basis, it appears that fibre-reinforced composites display not just creep and creep fracture strengths but even creep curve shapes which reflect the creep characteristics of the fibres incorporated for reinforcement.

These observations indicate that, with the Al_2O_{3f}/SiC samples, decaying primary stages are again due to gradual load transfer to stronger fibre regions. Yet, while matrix cracking accompanies creep of the longitudinal fibres, it appears that tertiary acceleration of the alumina fibres not matrix damage development initiates the tertiary stage in the Al_2O_{3f}/SiC composite. Although matrix cracking continues during the tertiary stage, for tests under vacuum, fibre failure begins only when the alumina fibres reach their limiting creep ductility under the test conditions imposed. Late during the tertiary life of the Al_2O_{3f}/SiC composite, progressive fibre failure then occurs rapidly until the stresses on the unbroken regions of the testpieces reach the levels required for sudden fracture by fibre pull out.

Unlike the various types of SiC fibres, alumina fibres might not be expected to be prone to oxidation-assisted fibre failure. However, oxidation can destroy the carbon coatings on the Al_2O_3 fibres, affecting creep ductility. This conclusion is verified by the fact that, at 100 MPa, the creep ductility of the Al_2O_{3f}/SiC material decreases from $\sim$0.10 to $\sim$0.01, with the rupture life decreasing from 2×10^5 s to 5×10^2 s, on changing the test atmosphere from vacuum to air.[7,8] Hence, for tests in air, matrix crack development again promotes oxygen penetration, with the consequent destruction of the carbon interfaces reducing the strains and times to failure.

4.3. Creep damage tolerance

In the absence of an appreciable tertiary stage, the woven SiC-fibre-reinforced composites must be defined as displaying creep-brittle behaviour,[23] i.e. $\varepsilon_r/\varepsilon_p \cong 1$, where ε_p is the total primary creep strain and ε_r is creep ductility. Then, since $(\varepsilon_r - \varepsilon_p) \cong 0$, near-zero values are also obtained for the 'creep damage tolerance' parameter (λ), given by[24]

$$\lambda = (\varepsilon_r - \varepsilon_p)/\dot{\varepsilon}_m.t_r \quad (4)$$

The creep damage tolerance value is important in practical situations when materials must withstand local strain concentrations, say, in regions where a change in component cross-section leads to stress concentrations. Values of λ in the range 5–10 are then thought to ensure that the strain concentrations encountered in service will not lead to premature failure.

Although large cracks can exist without causing immediate failure, with the woven SiC-fibre-reinforced materials, λ values close to zero represent a severe engineering design constraint. In contrast, with the Al_2O_{3f}/SiC product, well defined tertiary stages are observed.[7,8] Even when relatively low creep ductilities are exhibited during tests in air (with $\varepsilon_f \cong 0.01$), the recorded creep curves allow the λ values to be estimated as around 5. Clearly, from Figs. 1 and 3, the upper temperature limit of the alumina fibres reinforcing the Al_2O_{3f}/SiC composite is about 200 °C lower than the limits of the various SiC fibres used to produce the SiC-fibre-reinforced materials listed in Table 1. Nevertheless, the tertiary-dominated creep curves observed for the Al_2O_3-fibre-reinforced samples indicate the feasibility of producing future CFCMCs with the creep strength, oxidation resistance and creep damage tolerance levels required for high-performance aeroengine applications.

5. Conclusions

Comparisons of the creep and creep fracture properties of seven different CFCMCs show that, in all cases, the creep strengths of the fibres exceed those of the matrices. This conclusion contrasts with previous suggestions that the matrices are more creep resistant than the fibres reinforcing the Al_2O_{3f}/SiC composite,[7,8] the three SiC_f/SiC type products[4–6] and the SiC_f/RBSN material.[1]

For the broad product range considered, the longitudinal fibres control the rates of creep strain accumulation. Creep of the fibres is then accompanied by cracking of the porous matrices, with crack development also determined by the creep resistance of the longitudinal crack-bridging fibres. However, oxygen penetration into the testpieces during creep exposure can promote progressive failure of the crack-bridging

fibres, influencing the strains and times to fracture. Differences in the creep behaviour patterns observed for different CFCMCs therefore depend not only on the fibre reinforcement but also on factors such as the ease of oxygen ingress through the matrices and the oxidation resistance of the fibre/matrix interfaces.

References

1. Holmes, J. W. and Chermant, J. L., In: *Proc. 6th European Conf. on Composite Materials*, ed. R. Naslain, J. Lamon and D. Doumeingts. AMAC, Bordeaux, France, 1993, p. 633.
2. Birch, J. M., Wilshire, B. and Godfrey, D. J., *Proc. Br. Ceram. Soc*., 1978, **26**, 141.
3. Wilshire, B. and Carreño, F., *J. Eur. Ceram. Soc*., 2000, **20**, 463.
4. Zhu, S., Mizuno, M., Kagawa, Y., Cao, J., Nagano, Y. and Kaya, H., *Mater. Sci. Eng*., 1987, **A225**, 69.
5. Zhu, S., Mizuno, M., Nagano, Y., Cao, J., Kagawa, Y. and Kaya, H., *J. Am. Ceram. Soc*., 1998, **81**, 2269.
6. Zhu, S., Mizuno, M., Kagawa, Y., Cao, J., Nagano, Y. and Kaya, H., *J. Am. Ceram. Soc*., 1999, **82**, 117.
7. Lamouroux, F., Steen, M. and Vallés, J. L., *Comp. Sci. Technol*., 1996, **56**, 825.
8. Adami, J. N., *Comportement en Fluage Uniaxial Sous Vide d'un Composite 2D, Al_2O_3/SiC*. Thèse, Ecole Polytechnique de Zürich, 1992.
9. Newkirk, M. S., Urquhart, A. W., Zwicker, H. R. and Breval, E., *J. Mater. Res*., 1986, **1**, 81.
10. Newkirk, M. S., Lesher, H. D., White, D. R., Kennedy, C. R., Urquhart, A. W. and Clear, T. D., *Ceram. Eng. Sci. Proc*., 1987, **8**, 879.
11. Abe, Y., Horikiri, S., Fujimura, K. and Ichiki, E., In: *Progress in Sci. & Eng. of Composites*, ed. T. Hayashi, K. Kawata and S. Umekawa. Japan Soc. Comp. Mater., 1982, p. 1427.
12. Laffon, C., Flank, A. M., Lagarde, P., Laridjani, M., Hagege, R. and Olry, P. et al., *J. Mater. Sci*., 1989, **24**, 1503.
13. Bodet, R., Bourrat, X., Lamon, J. and Naslain, R., *J. Mater. Sci*., 1995, **30**, 661.
14. Chollon, G., Pailler, R., Naslain, R. and Olry, P., In *High Temperature Ceramic-Matrix Composites, II: Manufacturing and Materials Development*, ed. A.G. Evans and R. Naslain. Am. Ceram. Soc., Westerville, OH., 1995, p. 299.
15. Fox, D. S., *Ceram. Eng. Sci. Proc*., 1995, **16**, 877.
16. DiCarlo, J. A., *J. Mater.Sci*., 1986, **21**, 217.
17. O'Meara, C., Suihkonen, T., Hansson, T. and Warren, R., *Mater. Sci. Eng*., 1996, **A209**, 251.
18. Simon, G. and Bunsell, A. R., *J. Mater. Sci*., 1984, **19**, 3670.
19. Heredia, F. E., Evans, A. G. and Andersson, C. A., *J. Am. Ceram. Soc*., 1995, **78**, 2790.
20. Carter, C. H. Jr. and Davis, R. F., *J. Am. Ceram. Soc*., 1984, **67**, 732.
21. Bunsell, A. R. and Berger, M.-H., *J. Eur. Ceram. Soc*., 2000, **20**, 2249.
22. Davies, C. K. L. and Sinha Ray, S. L., In: *Special Ceramics*, Vol. 5. ed P. Popper. Br. Ceram. Res. Assoc., Stoke-on-Trent, 1972, p. 193.
23. Goodall, I. N., Leckie, F. A., Ponter, A. R. S. and Townley, C. H. A., *J. Eng. Mater. Tech*., 1979, **11**, 137.
24. Goodall, I. N., Cockcroft, R. D. H. and Chubb, E. J., *Int. J. Mech. Sci*., 1975, **17**, 351.